Remote Sens. **2014**, *6*, 1211-1233; doi:10.3390/rs6021211

OPEN ACCESS

remote sensing

ISSN 2072-4292

www.mdpi.com/journal/remotesensing

Article

The Generalized Difference Vegetation Index (GDVI) for Dryland Characterization †

Weicheng Wu

ICARDA (International Center for Agricultural Research in the Dry Areas), CGIAR, P.O. Box 950764, Amman 11195, Jordan; E-Mail: w.wu@cgiar.org; Tel.: +962-6-590-3120; Fax: +962-6-552-5930.

† This paper is an extension version of the paper presented in the 8th International Soil Sciences Congress (ISSC), Izmir, Turkey, 15–17 May 2012.

Received: 3 November 2013; in revised form: 24 December 2013 / Accepted: 2 January 2014 / Published: 29 January 2014

Abstract: A large number of vegetation indices have been developed and widely applied in terrestrial ecosystem research in the recent decades. However, a certain limitation was observed while applying these indices in research in dry areas due to their low sensitivity to low vegetation cover. In this context, the objectives of this study are to develop a new vegetation index, namely, the Generalized Difference Vegetation Index (GDVI), and to examine its applicability to the assessment of dryland environment. Based on the field investigation and crop Leaf Area Index (LAI) measurement, five spring and summer Landsat TM and ETM+ images in the frame with Path/Row number of 174/35, and MODIS (Moderate Resolution Imaging Spectroradiometer) LAI and vegetation indices (VIs) data (MOD15A2 and MOD13Q1), of the same acquisition dates as the Landsat images, were acquired and employed in this study. The results reveal that, despite the same level of correlation with the fractional vegetation cover (FVC) as other VIs, GDVI shows a better correlation with LAI and has higher sensitivity and dynamic range in the low vegetal land cover than other vegetation indices, e.g., the range of GDVI is higher than Normalized Difference Vegetation Index (NDVI),Soil-Adjusted Vegetation Index (SAVI), Enhanced Vegetation Index (EVI), Wide Dynamic Range Vegetation Index (WDRVI), and Soil-Adjusted and Atmospherically Resistant Vegetation Index (SARVI), by 164%–326% in woodland, 185%–720% in olive plantation, and 190%–867% in rangeland. It is, hence, concluded that GDVI is relevant for, and has great potential in, land characterization, as well as land degradation/desertification assessment in dryland environment.

Keywords: GDVI; LAI; vegetation indices; sensitivity; dynamic range; land characterization; dryland environment

1. Introduction

Spectral vegetation indices (VIs) are mathematical combinations of different spectral bands, mostly in the visible and near infrared regions of the electromagnetic spectrum [1,2], and are optical measures of vegetation canopy greenness, a composite property of leaf chlorophyll, leaf area, canopy cover, and canopy architecture [3]. Since the development of the Simple Ratio Index (SR) [4–6] and the Normalized Difference Vegetation Index (NDVI) [1,7], a number of vegetation indices, such as the Transformed Vegetation Index (TVI) [8], Perpendicular Vegetation Index (PVI) [9], Weighted Difference Vegetation Index (WDVI) [10,11], Non-Linear Vegetation Index (NLI) [12]), Green Red Vegetation Index (GRVI) [13,14], and Wide Dynamic Range Vegetation Index (WDRVI) [15], have been proposed. In addition, a certain number of indices taking the atmospheric effects and/or soil influence into account, namely, the Global Environmental Monitoring Index (GEMI) [16], Soil-Adjusted Vegetation Index (SAVI) [17], Transformed SAVI (TSAVI) [18], Modified SAVI (MSAVI) [19], Optimized SAVI (OSAVI) [20], Generalized SAVI (GeSAVI) [21], Green SAVI (GSAVI) [22], Modified Non-Linear Vegetation Index (MNLI) [23], Atmospherically Resistant Vegetation Index (ARVI), and Soil-Adjusted and Atmospherically Resistant Vegetation Index (SARVI) [24], SARVI2 [25], and later renamed as the Enhanced Vegetation Index (EVI) [26], and its two-band version (EVI2) [3], Green Atmospherically Resistant Index (GARI) [27], Visible Atmospherically Resistant Index (VARI) [13], *etc*., have been developed; and those frequently applied are listed in Table 1.

As well as these two-band and three-band indices, Kauth and Thomas [28], and Crist and Cicone [29,30], have developed the Tasseled Cap (TC) Transformation respectively for Landsat MSS (Multispectral Scanner System) and TM (Thematic Mapper) data. Recently, Huang *et al*. [31] have produced the TC coefficients for the ETM+ (Enhanced Thematic Mapper Plus) data. TC Transformation can provide different thematic information of land surface, namely, the Brightness (TCB), Greenness (TCG), and Wetness (TCW). The TCG is, in fact, an indicator of vegetation vigor or greenness, and was termed the Green Vegetation Index, a multiple linear spectral combination, e.g., four bands for MSS and six bands for TM and ETM+ data.

In terms of their development rationale, all of these indices, either ratio-based (SR, NDVI, SAVI, OSAVI, MSAVI, ARVI, GRVI, EVI, EVI2, *etc*.) or in the form of linear combination (PVI, WDVI, TVI, and TCG), were formulated on the basis of the strong contrast in reflectance between the near infrared (NIR) and red (R) bands as vegetation has strong reflection of the incident radiation in NIR band while a strong absorption in R band [1,15]. Considering the limitation or shortcoming of the most frequently applied NDVI, e.g., its saturation in densely vegetated area and its sensitivity to atmospheric effects and soil influence [13,15,17,24–26,32], a number of improved variants, such as SAVI, OSAVI, ARVI, SARVI, EVI, EVI2, and MNLI, have been derived to avoid the mentioned limitation by introducing either an adjustment factor (e.g., L in SAVI, SARVI, EVI, MNLI, EVI2), based on the soil line information or the blue band to correct the aerosol effect (e.g., ARVI, SARVI,

and EVI) or both the blue band and *L* (e.g., SARVI and EVI) to reduce both soil influence and atmospheric effects. All these vegetation indices have been widely applied and contributing to the ecosystem research and characterization by remote sensing, e.g., land cover classification, biomass and net primary production (NPP) quantification, crop yield estimation, land degradation monitoring, soil mapping, vegetation-climate interaction assessment, *etc*.

Table 1. Frequently applied vegetation indices developed in the past decades.

Index	Formula	Full Name	References
SR	ρ_{NIR}/ρ_R	Simple Ratio Index	[4–6]
NDVI	$(\rho_{NIR}-\rho_R)/(\rho_{NIR}+\rho_R)$	Normalized Difference Vegetation Index	[1,7]
PVI	$\sin(\alpha)(\rho_{NIR})-\cos(\alpha)(\rho_R)$ α = the angle between the soil line and NIR axis	Perpendicular Vegetation Index	[9]
TVI	$(\text{NDVI}+0.5)^{1/2}$	Transformed Vegetation Index	[8]
WDVI	$\rho_{NIR}-a\rho_R$ a = the slope of the soil line	Weighted Difference Vegetation Index	[10,11]
SAVI	$(1+L)(\rho_{NIR}-\rho_R)/(\rho_{NIR}+\rho_R+L)$ Low vegetation, L = 1, intermediate, 0.5, and high 0.25	Soil-Adjusted Vegetation Index	[17]
TSAVI	$a(\rho_{NIR}-a\rho_R-b)/[(a\rho_{NIR}+\rho_R-ab+X(1+a^2)]$ a = slope of the soil line, b = soil line intercept, and X = adjustment factor to minimize soil noise	Transformed Soil Adjusted Vegetation Index	[18]
OSAVI	$(\rho_{NIR}-\rho_R)/(\rho_{NIR}+\rho_R+0.16)$	Optimized Soil-Adjusted Vegetation Index	[20]
ARVI	$(\rho_{NIR}-\rho_{RB})/(\rho_{NIR}+\rho_{RB})$ $\rho_{RB}=\rho_R-\gamma\times(\rho_R-\rho_B)$ $\gamma=1$, ρ_B = reflectance of blue band	Atmospherically Resistant Vegetation Index	[24]
SARVI	$(1+L)(\rho_{NIR}-\rho_{RB})/(\rho_{NIR}+\rho_{RB}+L)$ ρ_{RB} is the same as that in ARVI, L is a correction factor similar to those of SAVI	Soil Adjusted and Atmospherically Resistant Vegetation Index	[24]
SARVI2 or EVI	$G\times((\rho_{NIR}-\rho_R)/(\rho_{NIR}+C1\times\rho_R-C2\times\rho_B+L))$ ρ_B = reflectance of blue band, G = 2.5, $C1$ = 6, $C2$ =7.5 and L = 1	Soil Adjusted and Atmospherically Resistant Vegetation Index 2 or Enhanced Vegetation Index	[25,26]
EVI2	$2.5(\rho_{NIR}-\rho_R)/(\rho_{NIR}+2.4\rho_R+L)$ L = 1	Enhanced Vegetation Index 2	[3]
NLI	$(\rho_{NIR}^2-\rho_R)/(\rho_{NIR}^2+\rho_R)$	Non-Linear Vegetation Index	[12]
MNLI	$(1+L)(\rho_{NIR}^2-\rho_R)/(\rho_{NIR}^2+\rho_R+L)$ L is a correction factor similar to those of SAVI	Modified Non-linear Vegetation Index	[23]
VARI	$(\rho_G-\rho_R)/(\rho_G+\rho_R-\rho_B)$ ρ_G= reflectance of the green band	Visible Atmospherically Resistant Index	[13]
WDRVI	$(a\times\rho_{NIR}-\rho_R)/(a\times\rho_{NIR}+\rho_R)$ a = 0.05–1, usually, 0.1–0.2	Wide Dynamic Range Vegetation Index	[15]

The main biophysical character of the dryland environment is its low vegetation cover (despite that it may be locally dense, e.g., in low-lying lands, riparian plains) due to aridity. According to the United Nations (UN) [33], the aridity index, the ratio of precipitation to potential evapotranspiration (denoted

as P/PET), of drylands, is between 0.05 and 0.65 (<550–600 mm of annual rainfall). Hence, such aridity (or water scarcity) affects food security, and, at the same time, makes land susceptible to degradation [33]. For this reason, a number of authors have conducted studies on monitoring of the vegetation condition and its change trend of and the impacts of anthropogenic activity on the vulnerable dryland environment either by using albedo [34,35] or by VIs, such as NDVI in combination with rainfall [36–40].

However, it was noted that even though some of these VIs have taken the soil and atmospheric influences into consideration, they are mostly sensitive to moderately and densely vegetated land cover, such as forests and croplands rather than to low vegetal drylands. Taking SAVI as an instance, Qi *et al*. [19] noted that, after introduction of the adjustment factor, *L*, the dynamic range of SAVI is reduced, which is not favorable for study in sparsely vegetated areas. In fact, not only SAVI, but also other indices, such as NDVI, EVI, and ARVI have low dynamic range in these areas. While conducting an assessment on the effectiveness of sand-control and land degradation in the Ordos Desert rangelands in China, using Landsat imagery, it came to the attention of the authors [40] that it was almost impossible to discern the subtle increase in greenness in the newly controlled areas (e.g., <4–5 years) based on the available vegetation indices due to their low dynamic range and insensitivity. Such insensitivity constitutes the limitation of these indices when applied to dryland research. Therefore, there is a need to develop another new vegetation index relevant for such low vegetation dryland environment.

The main objectives of this paper are to propose a new vegetation index and investigate its relevance for, sensitivity to, and applicability in low vegetation land cover in arid and semi-arid environment. A test site, located in the northwest of Syria, was selected to demonstrate the development and evaluation of the new index.

2. Materials and Methods

2.1. Rationale

While other authors use soil line information in the NIR–R space to derive vegetation indices [3,9–11,17,18,20,21,25,32], this paper attempts to generate a new index from the already popularized and frequently applied NDVI and SR. As Pinty and Verstraete [16] and Jackson and Huete [41] revealed, NDVI and SR can be converted from each other, that is,

$$NDVI = (SR - 1)/(SR + 1) \quad (1)$$

where $SR = \rho_{NIR}/\rho_R$, ρ_{NIR} and ρ_R are respectively reflectance of the NIR and R bands. Clearly, Equation (1) can be considered as a function of NDVI with respect to the variable SR, that is, any change in SR will lead to change in NDVI. However, for a given land cover, SR is fixed to certain extent and so is NDVI. If one wants to augment the value, *i.e.*, the dynamic range of NDVI of the given land cover type, the only possibility is to increase SR through certain operation, e.g., power operation, in the form of SR^n (n is an integer >0). A simple experiment using Landsat images reveals that through power operation (when n = 2, 3, and 4, for example), SR^n is to a varying degree amplified depending on land cover types and power number n (see Table 2). This implies that power operation on SR can lead to an amplification of the dynamic range of the new derivatives of NDVI (Table 2,

when $n > 1$). To facilitate the description, we term the new derivatives of NDVI the Generalized Difference Vegetation Index (GDVI), and mathematically, Equation (1) can be, thus, generalized as:

$$GDVI\hat{}n = (SR^n - 1)/(SR^n + 1) = (\rho_{NIR}^n - \rho_R^n)/(\rho_{NIR}^n + \rho_R^n) \quad (2)$$

where n is power, an integer of the values of 1, 2, 3, 4... n. The global dynamic range of GDVI is the same as NDVI, from −1 to 1; and, when $n = 1$, GDVI = NDVI. For facilitating the description, GDVI is denoted respectively GDVI^2, GDVI^3, and GDVI^4 when $n = 2$, 3, and 4.

In order to understand the characteristics of the new index, GDVI was projected against its origin, NDVI, taking the same images from which Table 2 was derived, as an example. The projection is shown in Figure 1. Two features of GDVI can be easily observed: (1) amplification of the dynamic range in the low and moderate vegetation cover with respect to NDVI, e.g., for a typical low vegetal rangeland/desert, NDVI is 0.2 but GDVI^2, GDVI^3, and GDVI^4 are respectively about 0.38, 0.54, and 0.67, a clear increase in the dynamic range (h in Figure 1a, 1b and 1c); and (2) saturation of the high power GDVI in the densely vegetated areas, e.g., GDVI^3 and GDVI^4 get saturated, respectively, when NDVI is >0.65 and >0.5 (the S point in Figure 1b,c).

Table 2. Atmospherically corrected and reflectance-based Simple Ratio Index (SR) and its derivatives ($n > 1$).

	N	Wheat	Forests	Woodlands	Olive Plantations	Rangelands	Bare Soil
SR^n	1	7.3547	3.5546	2.0720	1.4717	1.6564	1.3056
	2	52.9660	12.5400	4.2465	2.1771	2.7352	1.7012
	3	372.3832	43.7906	8.7200	3.2358	4.5014	2.2126
	4	2,805.4020	157.2514	18.0323	4.7398	7.4812	2.8942
$(SR^n - 1)/(SR^n + 1)$	1	0.7606	0.5609	0.3490	0.1908	0.2471	0.1325
	2	0.9629	0.8523	0.6188	0.3705	0.4645	0.2596
	3	0.9946	0.9553	0.7942	0.5278	0.6365	0.3775
	4	0.9993	0.9874	0.8949	0.6516	0.7642	0.4864

Figure 1. Characteristics of GDVI *vs*. NDVI ((**a**) GDVI^2 *vs.* NDVI, (**b**) GDVI^3 *vs.* NDVI and (**c**) GDVI^4 *vs*. NDVI).

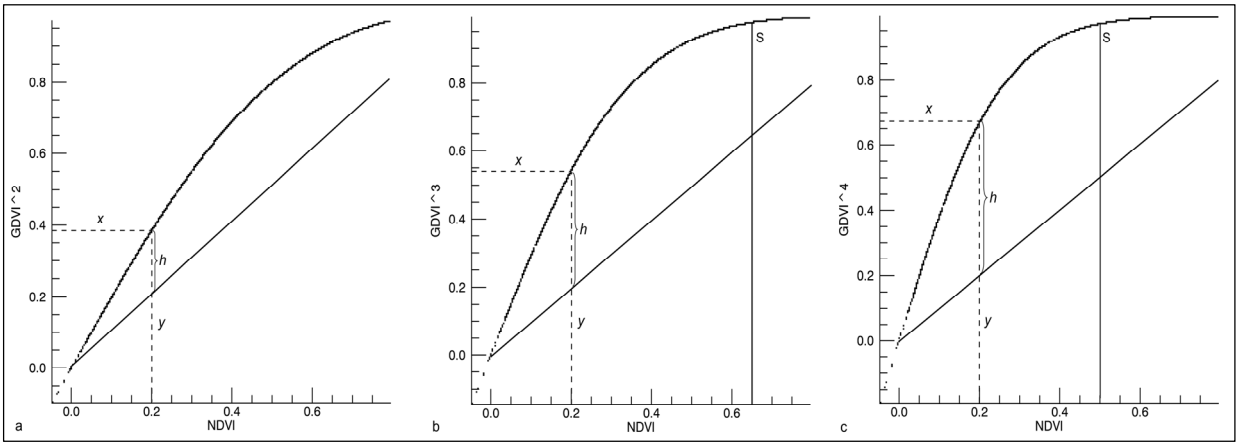

As Goel and Qin [12], Pinty and Verstraete [16], and Gong *et al*. [23] have explained, the relationships between different surface biophysical features often tend to be non-linear. Thus, the

objective of the non-linear operation is to linearize the relationships between the biophysical parameters [23]. However, the non-linear power operation in GDVI is not for such a linearization but for an enlargement of the contrast between the reflection in NIR (vegetation signal) and absorption in R bands. This is the reason that GDVI has a wider dynamic range in the low vegetation biome than NDVI and other ratio-based indices.

2.2. Test Site

To test and demonstrate the applicability and sensitivity of GDVI, an area located in northwestern Syria including a part of the governorates of Aleppo, Idleb, and Lattakia, covered by the Landsat frame/scene with Path/Row number 174/35 was selected (Figure 2). The landform in the test site is coastal slope and mountains with peak altitude of 1,500–1,710 m in the west, depression/valley in the middle (about 160–170 m in altitude), and plateau/plain with interspersed hills with an altitude range of 310–550 m (locally reaching 870 m) in the east. The area is dominated by Mediterranean climate with mean annual rainfall from 600 mm in the northwest to 200 mm in the southeast. The precipitation is mostly concentrated in winter and spring. These landscape and climatic characteristics constrain largely the diversity of land cover types and land use in agriculture, e.g., forest (mainly coniferous) and maquis (Mediterranean shrubland) in the mountainous chain, and on the slope, in the west, irrigated and rainfed croplands (wheat, barley, and vegetables) in spring, and irrigated cropland (e.g., cotton, maize, sesame, sunflower, watermelon) in summer in the valley and plateau, and rangeland/bare land in the low rainfall areas in the east. Permanent tree crops (mainly perennial olive tree crops, citrus/orchard including lemon, orange, fig, cherry, peach, and other fruit trees) are widely grown in rainfed areas crossing from the coastal slope to the depression/valley and then to the plateau in the east. The test site is one of the most important agricultural production areas in Syria, especially, known for its products of olive and wheat.

2.3. Data

Five spring and summer Landsat images, and MODIS LAI and EVI/NDVI including the reflectance of the B (blue), R, NIR, and MIR (middle infrared) bands corresponding to the acquisition dates of Landsat images were obtained and are listed in Table 3.

MODIS LAI was produced based on vegetation index, such as NDVI, directional spectral reflectance and radiative transfer models proposed by Myneni *et al*. [42], Knyazikhin *et al*. [43], and Myneni *et al*. [44]. The LAI products of collections 3 and 4 (C003 and C004) were generally found to have an overestimate compared to *in situ* observations [45,46], but the C005 product seems much more realistic, especially, for coniferous forest [47]. Land use/cover data were obtained, based on four field investigations, in the spring of 2007, 2009, 2010, and 2011, in the test site.

A limited number of LAI measurements, using AccuPAR Ceptometer (LP-80, Decagon Devices, Inc.) for wheat under supplemental irrigation and rainfed barley, were conducted in the campus of ICARDA (International Center for Agricultural Research in the Dry Areas), near Aleppo in Syria (see Figure 2 for location), during the peak growing period of wheat and barley from 10 to 15 April 2010, and from 21 to 31 March 2011.

Figure 2. Location of the test area.

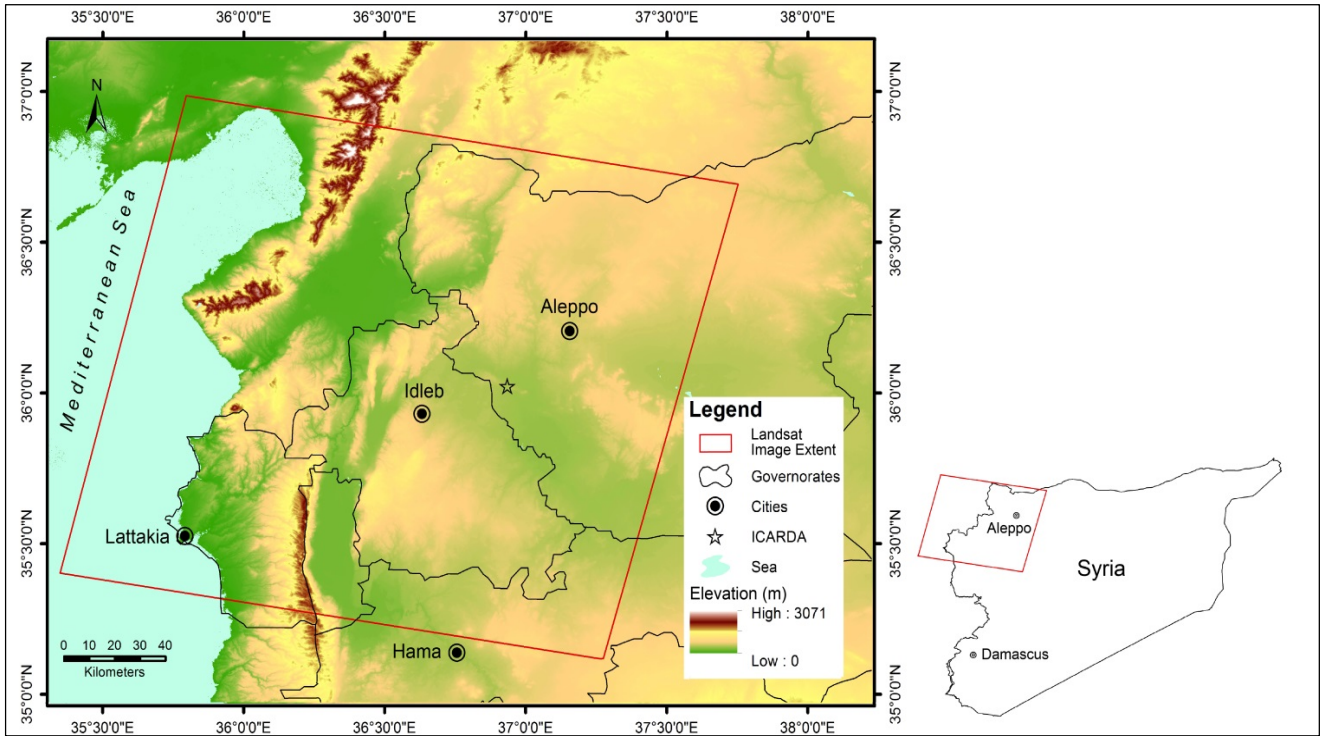

Table 3. Satellite data used in the study.

Acquisition Date of Landsat Images	MODIS Production Date (Including Day Of Year (DOY))	
(Path/Row: 174/35, 30 m)	**LAI (C005)** (MOD15A2, 8-day, 1,000 m)	**NDVI/EVI (C005)** (MOD13Q1, 16-day, 250 m)
27 March 2003 (ETM+)	22 March (81), and 29 March (89), 2003	81 (22 March), 97 (7 April)
1 May 2007 (TM)	23 April (113), 1 May (121) and 9 May (129), 2007	113 (23 April), 129 (09 May)
21 August 2007 (TM)	13 August (225), 21 August (233), and 29 August (241), 2007	225(13 August), 241 (29 August)
12 July 2010 (TM)	4 July (185), 12 July (193), and 20 July (201), 2010	193 (12 July)
29 August 2010 (TM)	21 August (233), 29 August (241), and 6 September (249), 2010	241 (29 August)

As experiment fields in the campus, cultivation of wheat, barley, and other crops, such as lentil, faba bean, oat, and coriander were interleaved from each other and often different from year to year for the same parcel of land due to rotation practices. The size of different cropland patches varies from 0.1 to 3 ha depending on the slope and location.

The AccuPAR readings were made in 12 plots (1 × 1 m^2 in size) distributed, respectively, in two parcels of wheat land where crop performance was visually distinguished good (two plots), intermediate (two plots), and relatively poor (two plots) in each parcel (<2 ha in size). Another 12 plots were measured in two tracts of rainfed barley (for harvesting), based on the same sampling scheme as wheat (six plots for each tract). Some sporadic measurements (five plots in total) were also made in irrigated barley, which is not common in Syria. All these measurements were undertaken during

noon-time, from 11:00 am to 1:30 pm, while it was sunny (cloud-free) in the spring 2010, and repeated in wheat and rainfed barley lands in 2011, but in different locations due to crop rotation.

It was noted that the maximum MODIS LAI of the ICARDA Campus dated 1 May 2007 was only 1.07–1.1, much lower than the measured values, 2.6 for irrigated wheat, 5.4 and 1.9, respectively, for irrigated and rainfed barley. It was, hence, considered better to use the average values of the measured LAI of the irrigated wheat (2.01) and rainfed barley for harvesting (1.46) to represent these two croplands in spring images for this study. However, there were no field measurement for other biomes, such as forest, woodland, and rangeland. To use MODIS LAI for other biomes in the successive calibration is the only choice despite of its coarse resolution.

2.4. Evaluation Procedure

As Gitelson [15], Gong *et al*. [23] and Richardson *et al*. [48], have demonstrated, to test the reliability and the efficiency of a vegetation index, a common approach is to calibrate the index with LAI crossing different biomes to ascertain their relationship.

Carlson and Ripley [49] reported that the scaled NDVI, *i.e.*, $(NDVI\text{-}NDVI_0)/(NDVI_S\text{-}NDVI_0)$, where $NDVI_0$ and $NDVI_S$ are, respectively, the NDVI values of bare soil and full vegetation cover (100%), is out of the influence of atmospheric effects. They recommended using its square to represent the fractional vegetation cover (FVC) for land surface studies. Gutman and Ignatov [50] proposed to use directly the scaled NDVI as FVC; and this was followed by Jiménez-Muñoz *et al*. [51], Zhang *et al*. [52], and Kallel *et al*. [53]. One of the advantages of FVC lies in its simplicity to be derived from satellite images, e.g., from NDVI [49,50,52], or from Spectral Mixing Analysis (SMA) [51], or from isoline parameterization in the NIR-R space [53].

Based on the above understanding, both LAI and FVC were used for evaluation of the relevance of GDVI. Moreover, Sirikul [54] found that the relation between the field measured LAI and MODIS NDVI/EVI is poor in semi-arid areas and broadleaf forest biomes. It will be interesting for us to examine the relationships between MODIS GDVI/NDVI/EVI with MODIS LAI for the observed biomes in the test area. The procedure to assess the relevance, sensitivity and applicability of GDVI is demonstrated as follows:

2.4.1. Atmospheric Correction

This correction was conducted for Landsat images using FLAASH (Fast Line-of-sight Atmospheric Analysis of Spectral Hypercubes) Model [55,56], which was developed based on the MODTRAN (MODerate resolution atmospheric TRANsmission) theory by the Air Force Research Laboratory, USA. This model can correct both additive and multiplicative atmospheric effects. The FLAASH reflectance of each band was rescaled to normal reflectance range from 0 to 1.

2.4.2. Calculation of Different Vegetation Indices and FVC

A number of vegetation indices namely NDVI, EVI, SAVI, OSAVI, SARVI, VARI, WDRVI, NLI, MNLI, and GDVI (n = 2, 3 and 4) were transformed from the multispectral bands. As Wu *et al*. [57] noted, most of the pixel values of VARI and WDRVI (e.g., a = 0.1 and 0.2) were negative in woodland

and rangeland. Similarly, it was found that not only VARI and WDRVI, but also NLI and MNLI (L = 0.5 for intermediate vegetation cover in semi-arid areas) have negative values in almost all biomes except for wheat cropland. For this reason, only the Landsat image dated 1 May 2007, was used to derive these indices for comparison.

FVC [50–53] was also derived from the NDVI of Landsat image, dated 1 May 2007, after fixing the values of $NDVI_0$ (=0.11) and $NDVI_S$ (=0.96).

For MODIS LAI (eight-day interval), taking that of 1 May 2007 as an instance, three dates of LAI, DOY (Day of Year) 113 (24 April), 121 (1 May) and 129 (9 May), were combined to compose a multi-band image. Then, a multi-band maximization algorithm [57] was applied to get the maximum value of each pixel from the three LAI images in order to have a cloud-free or cloud influence minimized LAI image.

For MODIS NDVI/EVI (16-day interval), only two dates (113 and 129) of data were available for 1 May. After combination, the same procedure as for MODIS LAI was followed to derive the cloud-free NDVI, EVI data for 1 May (121).

Apart from these two indices, the cloud-free GDVI^2 was also produced from the NIR and R reflectance bands of the same dataset as NDVI and EVI (MOD13Q1).

2.4.3. Selection of Sampling Areas

Based on the field investigation, the identified land cover types are forest, maquis (Mediterranean shrubland), woodland, spring croplands (irrigated wheat, rainfed barley for harvesting, rainfed barley for grazing), summer irrigated croplands (maize, cotton, and water melon), residue of spring crop after harvesting, permanent tree croplands (citrus, orchard, and olive plantation), rangelands, stone pits/mining sites, fallow, and bareland. Sampling areas in the form of polygons were first randomly defined in each land cover class in the color composites of Landsat images in making reference to the ground observation and Google Earth. They were defined as many as possible for each biome in order to have enough spatial representativeness, e.g., >3%–5% of the whole land cover class. Then, these polygons were adjusted and reshaped against MODIS LAI to avoid mixed and bad pixels (underestimation or no data) in MODIS LAI data. The adjusted polygons were considered as the sampling areas for the Landsat-MODIS image pair. The location of the polygons of the same biome may be slightly different from image pair to image pair due to the difference in acquisition dates, land use change (between spring and summer, and among different years), and due to mixed or bad pixels in MODIS LAI data. More concretely, each Landsat-MODIS pair has its own sampling areas for each land cover class.

The sampling areas take up about 3.6% on average in each biome class. The location and pixel number of the sampling areas before resizing (see next section) are shown in Figure 3 and Table 4 taking the image pair of 1 May 2007, as an example.

2.4.4. Calculation of the Mean Values and the Random Point Values of Different VIs in the Sampling Areas

In order to have more comparability between Landsat and MODIS data, a pixel resizing from 30 m to 250 m for Landsat VIs and from 1,000 m to 250 m for MODIS LAI was conducted using nearest

neighbor resampling. After importation of these images into ArcGIS, 890 random points were generated in the defined polygons in which samples were assigned to each land cover type, based on its importance in the test site (see Table 4); and the point values and biome mean values of all VIs including GDVI derived from different Landsat images and cloud-free LAI, NDVI, GDVI, and EVI from MODIS data were calculated for each land cover class, namely forest, maquis, woodland, rangeland, rainfed barley for grazing, and bare soil for the spring image pairs. In the summer image pairs, irrigated crops (cotton, watermelon, and sunflower) and spring crop residue left after harvesting were included, instead of wheat, rainfed barley for harvesting and grazing.

Figure 3. Distribution of the sampling areas taking the Landsat-MODIS image pair of 1 May 2007 as an example.

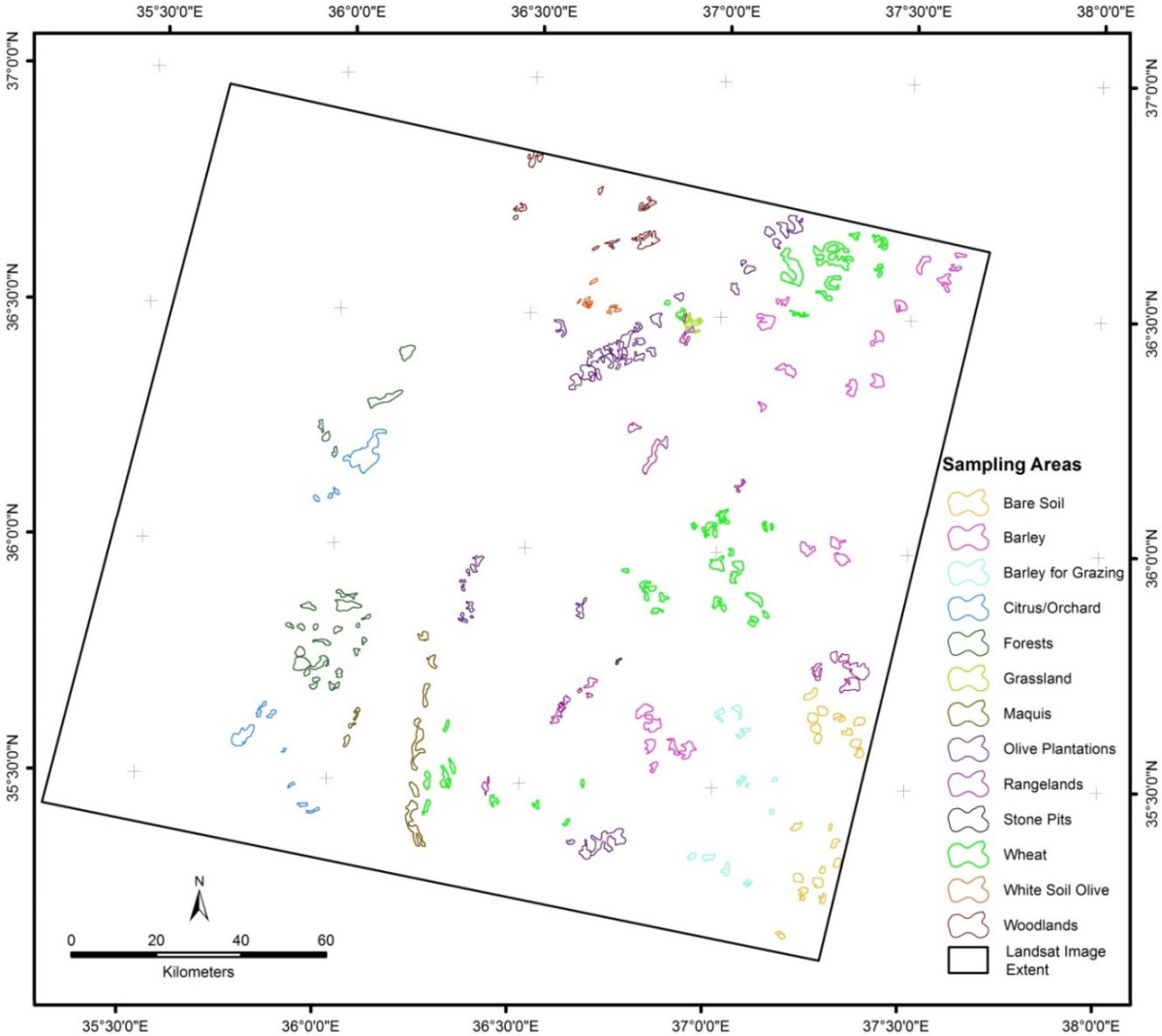

The mean FVC of 1 May 2007 was calculated for all biomes without pixel resizing as it will be directly calibrated with the VIs from the same Landsat images.

Table 4. Sampling areas before pixel resizing and random sample number in each land cover type taking the Landsat-MODIS pair of 1 May 2007 as an example.

Land Cover Types	Sampling Areas (in Pixels)			Randomly Sampling No
	Landsat TM/ETM+ (30 m)	MOD15A2 LAI (1,000 m)	MOD13Q1 NDVI/EVI (250 m)	
Forest	89,355	94	1,507	100
Maquis	54,410	75	918	50
Woodland	32,562	50	549	50
Olive	156,904	230	2,563	100
White Soil Olive	7,203	13	121	50
Citrus/Orchard	60,826	87	1,174	100
Irrigated Wheat	161,627	230	2,726	100
Barley for Harvesting	128,500	178	2,167	100
Barley for Grazing	24,979	34	421	50
Rangeland	80,799	63	1,163	100
Stone Mining	793	1	13	10
Grasslands	5,500	8	93	30
Bare Soil	71,078	94	1,199	50

2.4.5. Calibration

Landsat VIs *vs.* MODIS LAI: The studies conducted by Myneni *et al*. [42], Richardson *et al*. [48], Price and Bausch [58], and Gitelson *et al*. [59] revealed allometric relations between LAI and other vegetation indices, such as NDVI and WDRVI, which can be calibrated by either logarithmic or exponential or polynomial function. To compare the results, this calibration was conducted in two ways: (1) Random samples of LAI (from MODIS LAI without integration of field measured LAI) were linked with their corresponding VIs across all different land cover types; (2) the mean LAI values of different land cover were coupled with the mean VIs (using the measured mean LAI for wheat and rainfed barley). Both calibrations were conducted by simple linear regression model (least-square) at the confidence level of 95% after the conversion of LAI into different variants such as ln(LAI) and exp(LAI).

Landsat VIs *vs.* Landsat FVC: The mean VIs and GDVI of Landsat images dated 1 May 2007 were also coupled with the mean FVC and its exponential and logarithmic variants across all land cover types to check whether GDVI is better correlated with FVC than other indices.

MODIS VIs *vs.* MODIS LAI: The mean MODIS NDVI, EVI, and GDVI^2 were linked to the mean LAI from MOD15A2 across different land cover to check whether GDVI has better correlation with LAI than that of NDVI and EVI.

2.4.6. Sensitivity Analysis

Gitelson [15] has evaluated the sensitivity of WDRVI *vs*. NDVI. By following his approach, the sensitivity of the new vegetation index, GDVI, against other referenced VI can be quantitatively analyzed using the following expression:

$$S_r(GDVI) = [d(GDVI)/d(VI)] \times [\Delta(GDVI)/\Delta(VI)]^{-1} \quad (3)$$

where $S_r(GDVI)$ is the relative sensitivity of GDVI *vs*. the referenced VI (such as NDVI, EVI, SAVI and SARVI); $d(GDVI)/d(VI)$ are the first derivative of GDVI with respect to VI or the infinitesimal change in GDVI corresponding to that of VI; and $\Delta(GDVI) = GDVI_{max} - GDVI_{min}$ and $\Delta(VI) = VI_{max} - VI_{min}$ are the ranges of GDVI and VI, *i.e.*, the difference between the maximum and minimum GDVI and VI values of the same land cover observed in the image. In operation, $d(GDVI)$ and $d(VI)$, the tiny change in GDVI and VI can be obtained by measuring the GDVI and VI in the adjacent pixels, which have very tiny differences in values in the same land cover type.

According to Gitelson [15], if $S_r > 1$, the observed index, in our case, GDVI, is more sensitive than the referenced VI; if $S_r = 1$, they have the same sensitivity; and if $S_r < 1$, GDVI is less sensitive than the referenced VI.

3. Results and Discussions

Following the above procedures, the most relevant relationships either in logarithmic or exponential function between vegetation indices and LAI of the observed five pairs of images were established. It was noted that logarithmic functions, *i.e.*, VI–ln(LAI), have much higher correlation coefficients than those of exponential ones; so the former are listed in Tables 5 and 6. Those of the image pairs of 12 July 2010 and 1 May 2007 are presented in Figures 4 and 5; and the values of vegetation indices of some typical dryland biomes are presented in Table 7.

Table 5. Calibrated logarithmic relationships between vegetation indices (VIs) and Leaf Area Index (LAI) from 890 random samples across all land cover types taking the image pair of 1 May 2007 as an example.

Logarithmic Function	Estimation Error	Multiple R^2
GDVI^2 = 0.251ln(LAI) + 0.639	±0.113	0.793
GDVI^3 = 0.228ln(LAI) + 0.764	±0.110	0.769
GDVI^4 = 0.188ln(LAI) + 0.836	±0.101	0.729
NDVI = 0.242ln(LAI) + 0.514	±0.119	0.762
SAVI = 0.094ln(LAI) + 0.212	±0.064	0.626
SARVI = 0.151ln(LAI) + 0.213	±0.079	0.739
OSAVI = 0.132ln(LAI) + 0.276	±0.070	0.734
MNLI = 0.095ln(LAI) − 0.071	±0.053	0.711
EVI = 0.183ln(LAI) + 0.352	±0.115	0.660
WDRVI = 0.217ln(LAI) − 0.32	±0.119	0.721

Table 6. Calibrated biome mean-based logarithmic relationships between the vegetation indices and LAI.

Image Date	Logarithmic Function	Multiple R^2
27 March 2003	NDVI = 0.2146ln(LAI) + 0.4448	0.7426
	GDVI^2 = 0.2431ln(LAI) + 0.6941	0.7881
	GDVI^3 = 0.1965ln(LAI) + 0.82	0.7600
	GDVI^4 = 0.1438ln(LAI) + 0.8878	0.7036
	EVI = 0.1912ln(LAI) + 0.3885	0.5178
	SAVI = 0.1083ln(LAI) + 0.2732	0.4915
	SARVI = 0.1915ln(LAI) + 0.2919	0.6642

Table 6. *Cont.*

Image Date	Logarithmic Function	Multiple R^2
1 May 2007	NDVI = 0.1784ln(LAI) + 0.4071	0.8729
	GDVI^2 = 0.2346ln(LAI) + 0.6457	0.8830
	GDVI^3 = 0.2209ln(LAI) + 0.7687	0.8572
	GDVI^4 = 0.1873ln(LAI) + 0.8375	0.8199
	EVI = 0.1492ln(LAI) + 0.3528	0.7410
	SAVI = 0.0935ln(LAI) + 0.2514	0.7302
	SARVI = 0.1623ln(LAI) + 0.2574	0.8521
21 August 2007	NDVI = 0.1939ln(LAI) + 0.4185	0.9307
	GDVI^2 = 0.2737ln(LAI) + 0.6587	0.9547
	GDVI^3 = 0.2812ln(LAI)+ 0.7768	0.9432
	GDVI^4 = 0.2619ln(LAI) + 0.8404	0.9135
	EVI = 0.1729ln(LAI) + 0.374	0.7707
	SAVI = 0.1118ln(LAI) + 0.2627	0.8000
	SARVI = 0.1865ln(LAI) + 0.2729	0.8938
12 July 2010	NDVI = 0.1648ln(LAI) + 0.3878	0.8702
	GDVI^2 = 0.2274ln(LAI) + 0.6166	0.8758
	GDVI^3 = 0.2261ln(LAI) + 0.7356	0.8591
	GDVI^4 = 0.2013ln(LAI) + 0.8048	0.8334
	EVI = 0.146ln(LAI) + 0.3541	0.6227
	SAVI = 0.0967ln(LAI) + 0.2579	0.6405
	SARVI = 0.1595ln(LAI) + 0.2435	0.7598
29 August 2010	NDVI = 0.1761ln(LAI) + 0.3955	0.8983
	GDVI^2 = 0.248ln(LAI) + 0.6268	0.9319
	GDVI^3 = 0.2538ln(LAI) + 0.7454	0.9255
	GDVI^4 = 0.2338ln(LAI) + 0.8105	0.8921
	EVI = 0.1527ln(LAI) + 0.3459	0.7365
	SAVI = 0.0989ln(LAI) + 0.2469	0.7568
	SARVI = 0.1698ln(LAI) + 0.2461	0.8656

Table 7. Values of vegetation indices of some typical biomes (Landsat image dated 1 May 2007).

VIs	Forest	Woodland	Citrus	Wheat	Barley	Olives	Grassland	Range-Land	Bare Land
GDVI^2	0.815	0.745	0.819	0.916	0.721	0.398	0.674	0.366	0.257
GDVI^3	0.933	0.890	0.930	0.975	0.865	0.550	0.838	0.511	0.375
GDVI^4	0.976	0.953	0.971	0.991	0.933	0.670	0.922	0.624	0.480
NDVI	0.522	0.453	0.536	0.678	0.440	0.212	0.390	0.193	0.131
EVI	0.399	0.353	0.512	0.674	0.349	0.145	0.337	0.169	0.120
SAVI	0.267	0.254	0.341	0.457	0.268	0.120	0.246	0.134	0.109
SARVI	0.350	0.292	0.395	0.521	0.273	0.093	0.255	0.072	−0.023
OSAVI	0.322	0.295	0.373	0.487	0.300	0.138	0.271	0.141	0.104
NLI	−0.227	−0.262	−0.025	0.282	−0.214	−0.557	−0.266	−0.434	−0.370
MNLI	−0.041	−0.060	−0.006	0.094	−0.058	−0.143	−0.080	−0.175	−0.208
WDRVI (a = 0.20)	−0.216	−0.302	−0.191	0.042	−0.307	−0.526	−0.372	−0.541	−0.587

Figure 4. Logarithmic relationships between vegetation indices and LAI (image pair dated 12 July 2010).

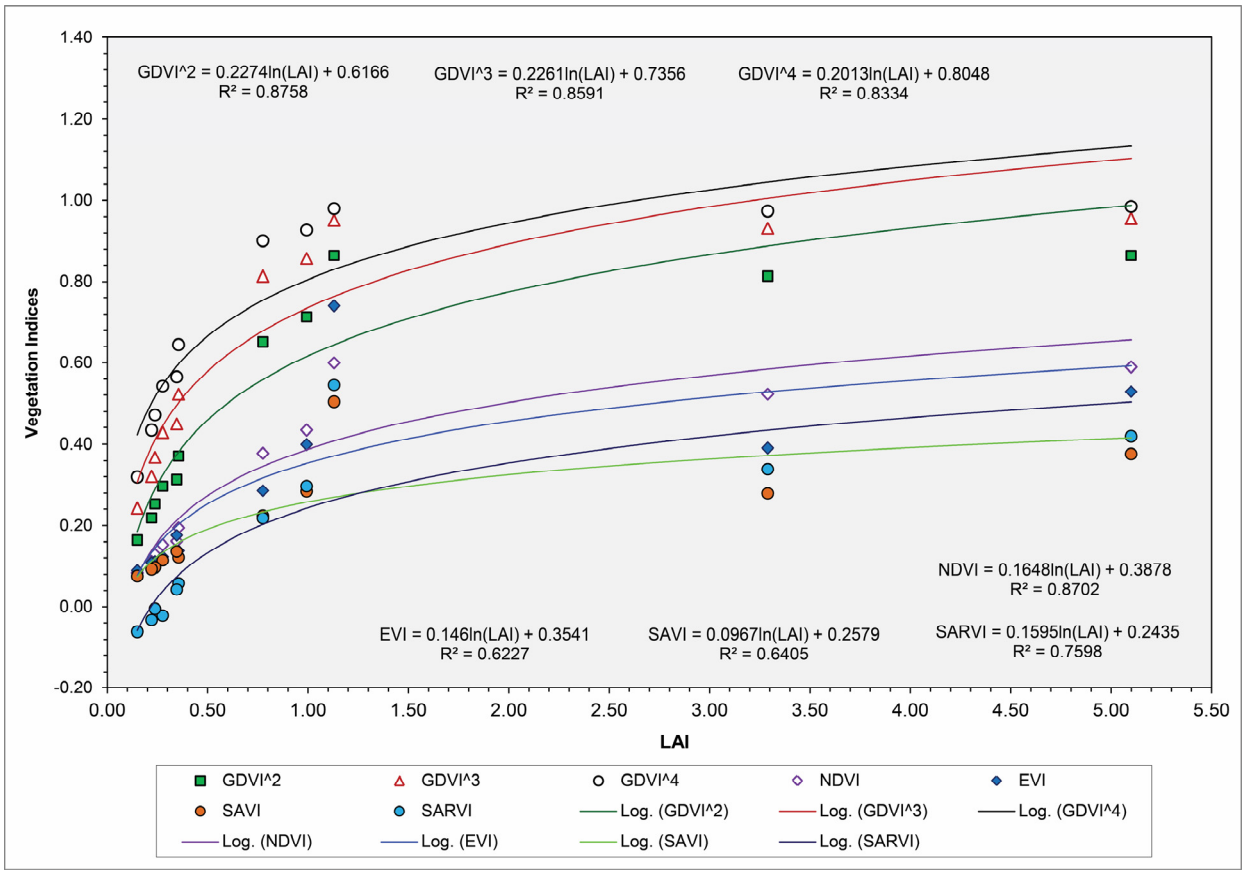

Figure 5. Logarithmic relationships between vegetation indices and LAI (image pair dated 1 May 2007. (**a**) GDVI *vs.* LAI, (**b**) VIs with positive range *vs*. LAI, and (**c**) VIs with negative range *vs*. LAI).

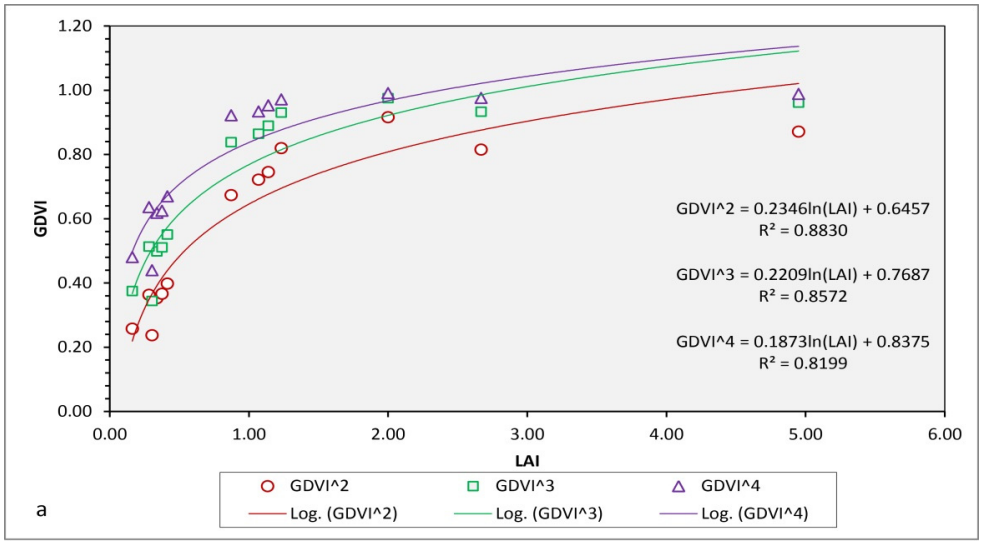

Figure 5. *Cont.*

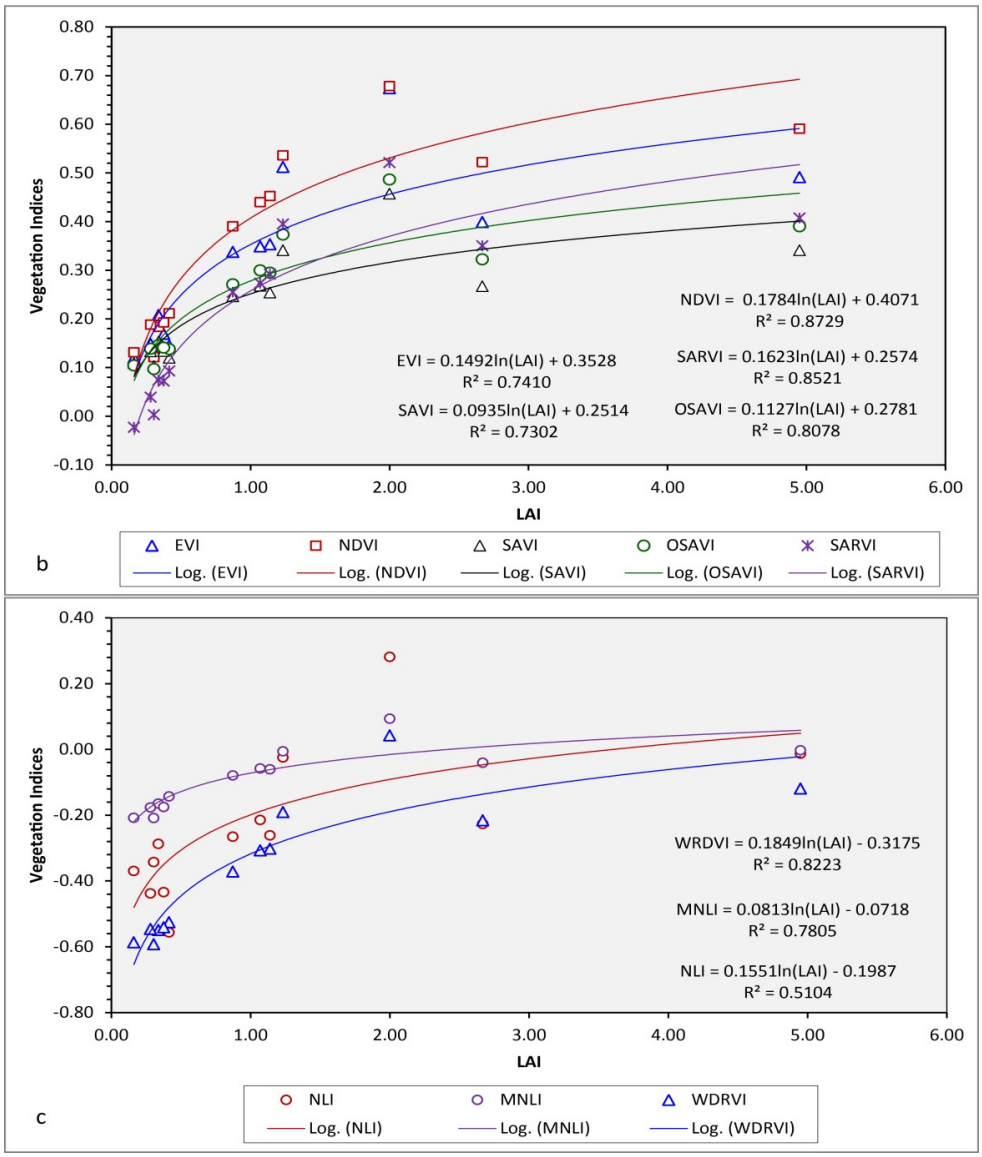

3.1. GDVI vs. LAI

3.1.1. Advantages

Better correlation with LAI than other indices: It is evident that both random point-based (Table 5) and biome mean-based (Table 6, Figures 4 and 5) calibrations illustrate that GDVI^2 is better correlated with LAI than any other index, such as NDVI, EVI, SAVI, OSAVI, SARVI, NLI, MNLI, and WDRVI across all land cover types. GDVI^3 and GDVI^4 are more or less at the same level as NDVI and SARVI, depending on images. Moreover, the correlation with LAI resulted from biome mean-based calibration (1 May 2007, in Table 6) is higher than that from random point-based calibration (Table 5), probably resulting from the sample mixing among different biomes in the latter while modeling was conducted.

As mentioned earlier, despite of the consideration of the "non-linear" factor in WDRVI (*i.e.*, $a \times \rho_{NIR}$), NLI and MNLI (*i.e.*, square of ρ_{NIR}), their values in most dryland biomes are negative (Figure 5c and Table 7). These indices are more applicable to study of densely vegetated areas, for

example, forests and croplands, rather than dryland areas, as one may not be used to seeing all negative values of a vegetation index crossing all land cover types.

Amplification of the dynamic range: As already discerned in Section 2.1, this advantage of GDVI, *i.e.*, amplification of the dynamic range in the low vegetated areas is obvious. As revealed in Table 7, the values of GDVI are magnified respectively by 164%–326%, 185%–720%, 190%–867%, and 196%–2,088% for the biomes namely woodland, olive plantation, rangeland, and bareland, in comparison with NDVI, SAVI, EVI, SARVI, NLI, MNLI, and WDRVI. This implies that GDVI gains more dynamic range for low vegetal biomes than other vegetation indices.

3.1.2. Sensitivity

Based on the measurements, such as tiny change, maximum, and minimum values of VIs and GDVI in the image dated 1 May 2007, the relative sensitivity of GDVI *vs*. other VIs across different biomes were calculated and are presented in Figure 6.

Figure 6. Sensitivity of GDVI *vs*. other vegetation indices for different biomes (image dated 1 May 2007. (**a**) GDVI^2 *vs.* VIs, (**b**) GDVI^3 *vs.* VIs, and (**c**) GDVI^4 *vs*. VIs).

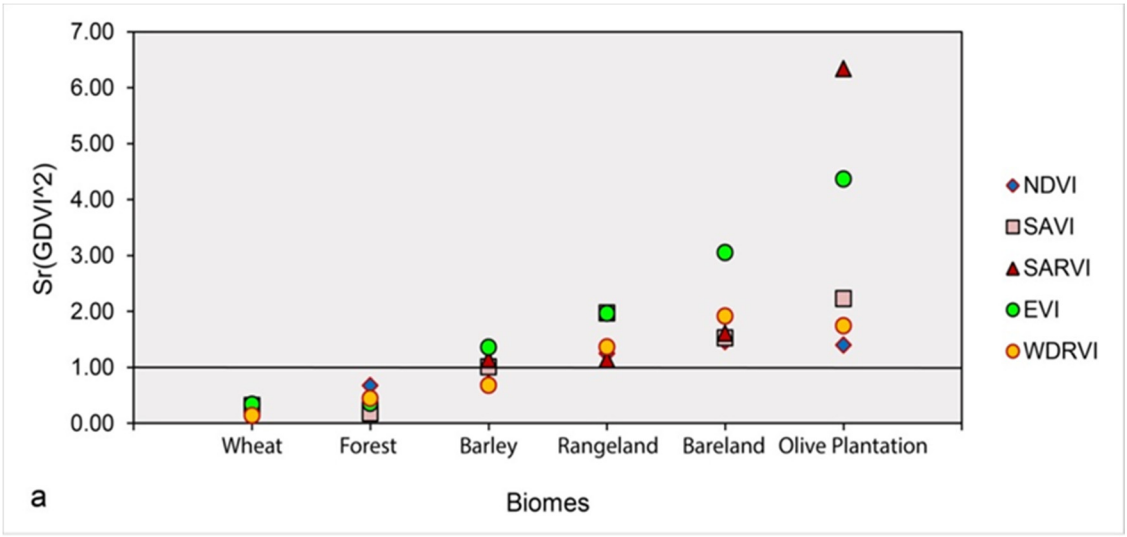

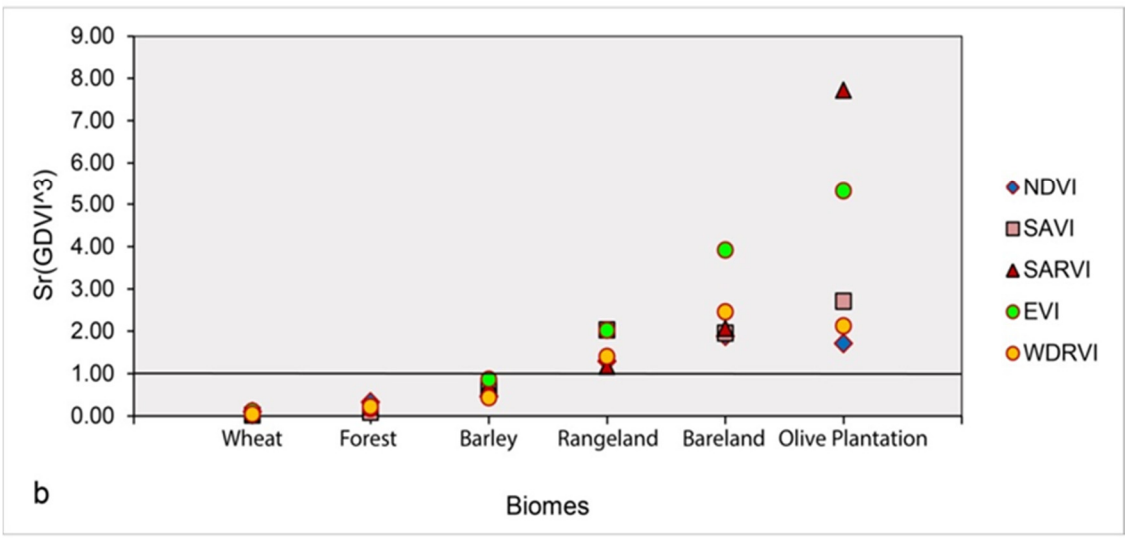

Figure 6. *Cont.*

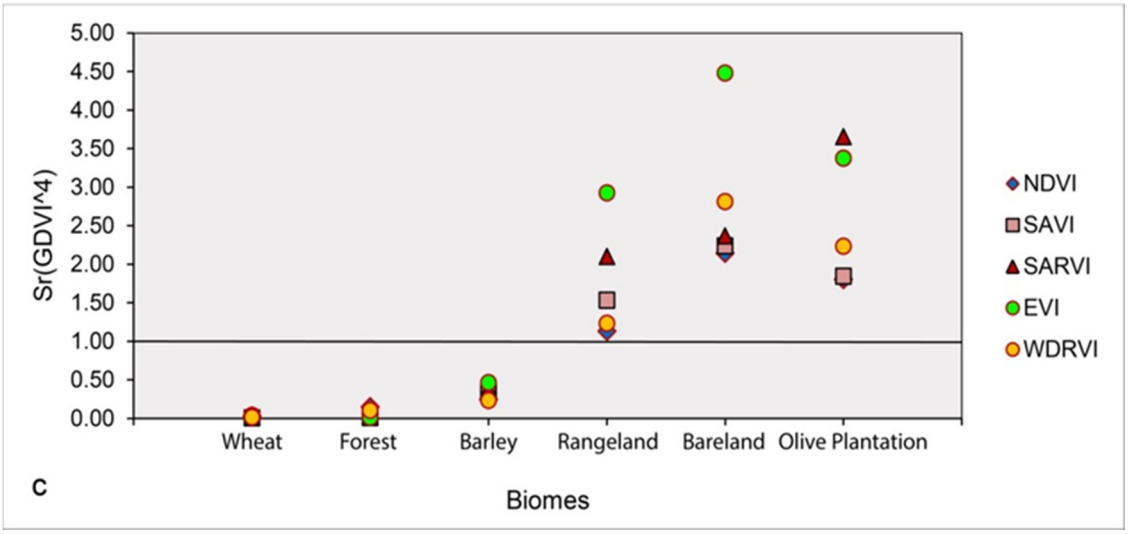

It is easily seen in Figure 6 that, for the biomes wheat and forest, the relative sensitivity, $S_r(GDVI)$, with respect to other vegetation indices is <1, implying that all power GDVI is less sensitive than other vegetation indices in the densely vegetated biomes. For rainfed barley, GDVI^2 has more or less similar sensitivity to others (Figure 6a). However, for the biomes rangeland, bareland, and olive groves, $S_r(GDVI) > 1$, indicating that GDVI has higher sensitivity than other vegetation indices in the sparsely vegetated areas.

3.2. GDVI vs. *FVC*

Together with other vegetation indices, GDVI was checked against FVC across all land cover types, and the results are listed in Table 8.

It is seen that, among the VI-FVC relationships, GDVI^2 is at the same level of correlation as NDVI, SARVI, EVI, WDRVI, among which, OSAVI is the best. As for VI-ln(FVC), GDVI^2 is the same as NDVI but GDVI^4 is the best. Among the VI-exp(FVC) functions, WDRVI, show better correlation than GDVI.

Table 8. Pearson correlation coefficients (R^2) between VIs/Generalized Difference Vegetation Index (GDVI) and fractional vegetation cover (FVC) from Landsat imagery dated 1 May 2007.

	SARVI	SAVI	OSAVI	EVI	NLI	MNLI	NDVI	WDRVI	GDVI^2	GDVI^3	GDVI^4
FVC	0.9663	0.9120	0.9821	0.9428	0.8172	0.9526	0.9683	0.9781	0.9683	0.9044	0.8336
ln(FVC)	0.7674	0.6496	0.7465	0.6626	0.4543	0.7500	0.8761	0.6773	0.8761	0.9332	0.9624
exp(FVC)	0.9624	0.9370	0.9841	0.9663	0.8686	0.9624	0.9197	0.9980	0.9197	0.8336	0.7534

3.3. MODIS GDVI vs. *MODIS LAI*

The evaluation of MODIS GDVI, EVI and NDVI *vs*. MODIS LAI (without integration of the field measurement), taking again the cloud-free MODIS data of 1 May 2007 as an example, reveals that all three vegetation indices are well correlated with the logarithmic variant of MODIS LAI if all observed

land cover types are taken into account; and NDVI is the best one followed by GDVI^2 (Figure 7). MODIS NDVI and EVI are poorly correlated with the field measured LAI [53], but MODIS GDVI, NDVI, and EVI are highly correlated with MODIS LAI, especially NDVI and GDVI.

Figure 7. Relationships between MODIS Normalized Difference Vegetation Index (NDVI), Enhanced Vegetation Index (EVI) and GDVI and MODIS LAI (1 May 2007).

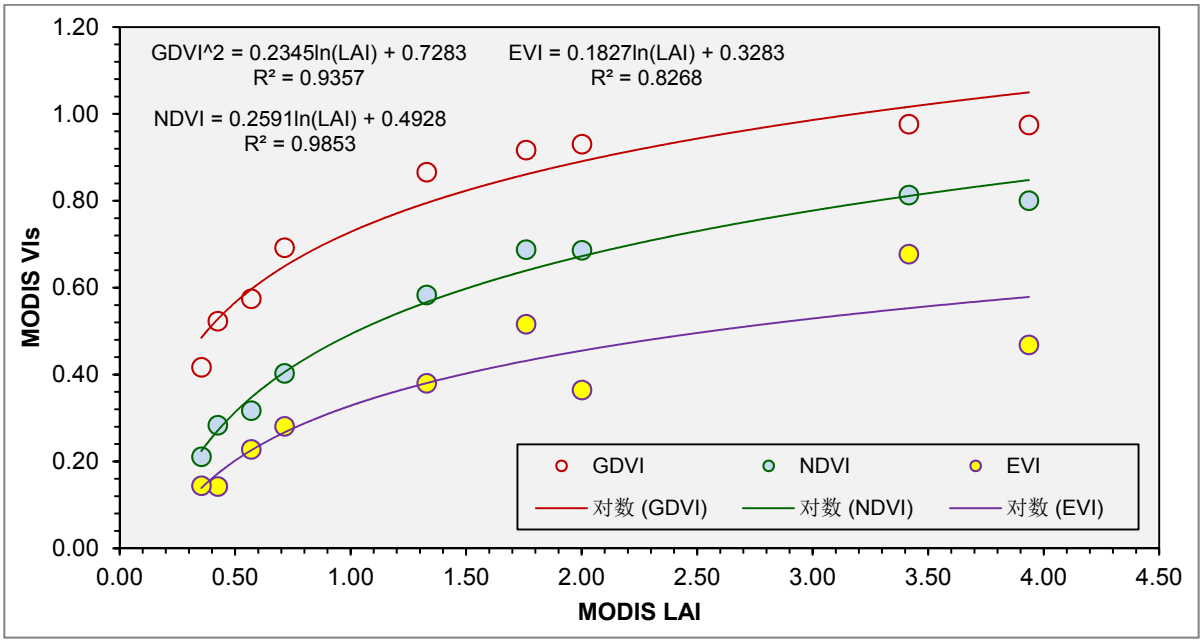

3.4. Discussion on Limitation and Problems Encountered

Despite of the advantages, the limitation of GDVI is also clear. Apart from the saturation, as raised in Section 2.1 and Table 7, GDVI has low sensitivity in the densely vegetated biomes, e.g., forest, maquis, irrigated croplands (e.g., wheat), as shown in Figure 6. The applicability of GDVI of different power is summarized in Table 9.

Problems were encountered in this study. Due to limited field measurements, MODIS LAI data have to be used for the non-measured biomes. As concerned by some authors [45–47,53], the quality of MODIS LAI eight-day product relies heavily on the weather condition in subtropical areas; especially, it is difficult to have completely cloud-free condition during the crop-growing period in spring. For this reason, underestimation may arise. Another factor influences the quality of MODIS LAI data lies in, perhaps, its biome mapping [44]. If a higher-resolution biome map is available, we believe that more relevant MODIS LAI product will be made available. In this study, the multi-date LAI maximization procedure can minimize, more or less, the problem related to cloud cover or bad pixels but cannot remove that resulted from biome mapping. Another shortcoming of MODIS LAI for such calibration is its coarse resolution. Clearly, it is not ideal to match VIs of 30 m resolution to LAI of 1,000 m resolution. Both degradation of 30 m VIs to 1000 m resolution and upgrading of 1000 m LAI to 30 m resolution will lead to either a loss or an unrealistic improvement in quality of the data. A feasible compromise is to degrade 30 m data to 250 m, and to upgrade 1,000 m LAI to 250 m as done in this study. It is worthy of mentioning that, for such study involving multi-resolution and multi-source data, selection of a reasonable resampling approach is also important. It is known that

both bilinear and cubic convolution resampling will change the original value of pixel due to an averaging of the observed pixel with its adjacent pixels. Thus, the best choice is to use the nearest neighbor resampling, in which the original values of pixels can be kept after pixel resizing.

Table 9. Applicability of GDVI.

GDVI	Land Cover Types								
	Forest/ Maquis	Irrigated Cropland	Wood-Lands	Citrus/ Orchard	Rainfed Cropland	Olive Plantation	Rangeland	Desert	Bare Land
GDVI^2	Partly, Yes	Partly, Yes	Yes	Yes	Yes	Yes	Yes	Yes	Yes
GDVI^3	No	No	Yes	Yes	Yes	Yes	Yes	Yes	Yes
GDVI^4	No	No	Partly, Yes	Partly, Yes	Partly, Yes	Yes	Yes	Yes	Yes

Moreover, limited field measurements do not allow us to assess whether field LAI is better than MODIS LAI for such calibration. The equations in Table 5 were obtained from 890 random samples but their correlation is lower than that of biome mean-based equations presented in Table 6, which are a result of the mixed LAI (field measured ones were used for wheat and rainfed barley while MODIS LAI for other land cover types). With the increase of the field measurement, field LAI-based calibration will be made possible. This can be a follow-up topic of research in the future.

FVC is a choice for calibration. As it is derived directly from NDVI and has a good linear correlation with most of the vegetation indices; and GDVI shows a better correlation with it only in logarithmic function.

4. Conclusions

This paper presented the development of the new vegetation index, GDVI, and explored its relevance for and applicability in dryland ecosystem research. Although more additional work, e.g., calibration and verification with more field measurements in different areas, is still needed, based on the conducted random sample-based and biome mean-based calibrations, we can already see that the proposed index has its uniqueness different from and advantages over other vegetation indices, *i.e.*, higher sensitivity and dynamic range in the low vegetal biomes in spite of its disadvantage and limitation (e.g., low sensitivity and saturation) in densely vegetated areas. Additionally, GDVI^2 seems able to catch better LAI than other VIs across different land cover types. Broadly speaking, GDVI^2 is mainly operational for land characterization in dryland biomes but, if applied to forest, shrubland, and cropland studies, care has to be taken due to its low sensitivity to these biomes. The higher power GDVI (n = 3, 4) is only applicable in sparsely vegetated areas, e.g., for monitoring land degradation and desertification in dryland ecosystems. After an extensive validation, GDVI can serve as a complement of the other vegetation indices for research in the dry areas. In the future, it is also possible to integrate GDVI into MODIS products and serve for dryland system research.

In this study, atmospheric effects have been considered in image preprocessing; however, soil influence has not been yet. As well as calibration in different dry areas, future work should take this correction into account as either done by Wang *et al*. [60] by applying the FFT (Fast Fourier Transform) to remove the background noise, or by Huete [17], Rondeaux *et al*. [20], and Gong *et al*. [23], by using a self-correction factor in different magnitude adapted to the power of GDVI.

Acknowledgments

Four Landsat images dated 27 March 2003, 21 August 2007, 12 July 2010, 29 August 2010, and all MODIS data (MOD15A2, MOD13Q1) were freely obtained from the USGS data server (http://glovis.usgs.gov/).

Conflicts of Interest

The author declares no conflict of interest.

References

1. Tucker, C.J. Red and photographic infrared linear combinations for monitoring vegetation. *Remote Sens. Environ.* **1979**, *8*, 127–150.
2. Vina, A.; Gitelson, A.A.; Nguy-Robertson, A.L.; Peng, Y. Comparison of different vegetation indices for the remote assessment of green leaf area index of crops. *Remote Sens. Environ.* **2011**, *115*, 3468–3478.
3. Jiang, Z.; Huete, A.R.; Didan, K.; Miura, T. Development of a two-band enhanced vegetation index without a blue band. *Remote Sens. Environ.* **2008**, *112*, 3833–3845.
4. Birth, G.S.; McVey, G.R. Measuring the color of growing turf with a reflectance spectrophotometer. *Agron. J.* **1968**, *60*, 640–643.
5. Jordan, C.F. Derivation of leaf-area index from quality of light on the forest floor. *Ecology* **1969**, *50*, 663–666.
6. Knipling, E.B. Physical and physiological bases for the reference of visible and near infrared radiation from vegetation. *Remote Sens. Environ.* **1970**, *1*, 155–159.
7. Rouse, J.W.; Haas, R.H.; Schell, J.A.; Deering, D.W. Monitoring Vegetation Systems in the Great plains with ERTS. In Proceedings of the 3rd ERTS-1 Symposium NASA SP-351, Washington, DC, USA, 10–14 December 1973; Volume 1, pp. 309–317.
8. Deering, D.W.; Rouse, J.W.; Haas, R.H.; Schel, J.A. Measuring Forage Production of Grazing Units from Landsat MSS Data. In Proceedings of the 10th International Symposium of Remote Sensing of Environment, Ann Arbor, MI, USA, 6–10 October 1975; Volume II, pp. 1169–1178.
9. Richardson, A.J.; Wiegand, C.L. Distinguishing vegetation from soil background information. *Photogramm. Eng. Remote Sens.* **1977**, *43*, 1541–1552.
10. Clevers, J.G.P.W. The derivation of a simplified reflectance model for the estimation of leaf area index. *Remote Sens. Environ.* **1988**, *35*, 53–70.
11. Clevers, J.G.P.W. Application of the WDVI in estimating LAI at the generative stage of barley. *ISPRS J. Photogramm. Remote Sens.* **1991**, *46*, 37–47.
12. Goel, N.S.; Qin, W. Influences of canopy architecture on relationships between various vegetation indices and LAI and FPAR: A computer simulation. *Remote Sens. Rev.* **1994**, *10*, 309–347.
13. Gitelson, A.A.; Kaufman, Y.J.; Stark, R.; Rundquist, D. Novel algorithms for remote estimation of vegetation fraction. *Remote Sens. Environ.* **2002**, *80*, 76–87.
14. Motohka, T.; Nasahara, K.N.; Oguma, H.; Tsuchida, S. Applicability of green-red vegetation index for remote sensing of vegetation phenology. *Remote Sens.* **2010**, *2*, 2369–2387.

15. Gitelson, A.A. Wide dynamic range vegetation index for remote quantification of crop biophysical characteristics. *J. Plant Physiol.* **2004**,*161*, 165–173.
16. Pinty, B.; Verstraete, M.M. GEMI: A non-linear index to monitor global vegetation from satellites. *Plant Ecol.* **1992**, *101*, 15–20.
17. Huete, A.R. A soil adjusted vegetation index (SAVI). *Remote Sens. Environ.* **1988**, *25*, 295–309.
18. Baret, F.; Guyot, G.; Major, D. TSAVI: A Vegetation Index which Minimizes Soil Brightness Effects on LAI and APAR Estimation. In Proceedings of the 12th International Canadian Symposium Geoscience and Remote Sensing (IGARSS'89), Vancouver, BC, Canada, 10–14 July 1989; pp. 1355–1358.
19. Qi, J.; Chehbouni, A.; Huete, A.R.; Kerr, Y.H.; Sorooshian, S. A modified soil adjusted vegetation index. *Remote Sens. Environ.* **1994**, *48*, 119–126.
20. Rondeaux, G.; Steven, M.; Baret, F. Optimization of soil-adjusted vegetation index. *Remote Sens. Environ.* **1996**, *55*, 95–107.
21. Gilabert, M.A.; Gonzalez-Piqueras, J.; Garcia-Haro, F.J.; Melia, J. A generalized soil-adjusted vegetation index. *Remote Sens. Environ.* **2002**, *82*, 303–310.
22. Sripada, R.P.; Heiniger, R.W.; White, J.G.; Meijer, A.D. Aerial color infrared photography for determining early in-season nitrogen requirements in corn. *Agron. J.* **2006**, *98*, 968–977.
23. Gong, P.; Pu, R.; Biging, G.S.; Larrieu, M.R. Estimation of forest leaf area index using vegetation indices derived from Hyperion hyperspectral data. *IEEE Trans. Geosci. Remote Sens.* **2003**, *41*, 1355–1362.
24. Kaufman, Y.J.; Tanré, D. Atmospherically resistant vegetation index (ARVI) for EOS-MODIS. *IEEE Trans. Geosci. Remote Sens.* **1992**, *30*, 261–270.
25. Huete, A.R.; Liu, H.Q.; Batchily, K.; van Leeuwen, W. A comparison of vegetation indices global set of TM images for EOS-MODIS. *Remote Sens. Environ.* **1997**, *59*, 440–451.
26. Huete, A.; Didan, K.; Miura, T.; Rodriguez, E.P.; Gao, X.; Ferreira, L.G. Overview of the radiometric and biophysical performance of the MODIS vegetation indices. *Remote Sens. Environ.* **2002**, *83*, 195–213.
27. Gitelson, A.; Kaufman, Y.; Merzlyak, M. Use of a green channel in remote sensing of global vegetation from EOS-MODIS. *Remote Sens. Environ.* **1996**, *58*, 289–298.
28. Kauth, R.J.; Thomas, G.S. The Tasseled Cap—A Graphical Description of the Spectral-Temporal Development of Agricultural Crops as Seen by Landsat. In Proceedings of the Symposium on Machine Processing of Remotely Sensed Data, Purdue University, West Lafayette, IN, USA, 29 June–1 July 1976; pp. 4B41–4B51.
29. Crist, E.P.; Cicone, R.C. Application of the tasseled cap concept to simulated thematic mapper data. *Photogramm. Eng. Remote Sens.* **1984**, *50*, 343–352.
30. Crist, E.P.; Cicone, R.C. A Physically-based transformation of thematic mapper data—The TM tasseled cap. *IEEE Trans. Geosci. Remote Sens.* **1984**, *22*, 256–263.
31. Huang, C.; Wylie, B.; Yang, L.; Homer, C.; Zylstra, G. Derivation of a tasseled cap transformation based on Landsat 7 at-satellite reflectance. *Int. J. Remote Sens.* **2002**, *23*, 1741–1748.
32. Baret, F.; Jacquemoud, S.; Hanocq, J.F. The soil line concept in remote sensing. *Remote Sens. Rev.* **1993**, *7*, 65–82.

33. United Nations (UN). Global Drylands: A UN System-Wide Response, 2011. Available online: http://www.unccd.int/Lists/SiteDocumentLibrary/Publications/Global_Drylands_Full_Report.pdf (accessed on 8 February 2012).
34. Courel, M.-F.; Kandel, R.S.; Rasool, S.I. Surface albedo and the Sahel drought. *Nature* **1984**, *307*, 528–531.
35. Otterman, J.; Tucker, C.J. Satellite measurements of surface albedo and temperatures in semi-desert. *J. Appl. Meteorol.* **1985**, *24*, 228–234.
36. Malo, A.R.; Nicholson, S.E. A study of rainfall and vegetation dynamics in the African Sahel using Normalized Difference Vegetation Index. *J. Arid Environ.* **1990**, *19*, 1–24.
37. Tucker, C.J.; Dregne, H.E.; Newcomb, W.W. Expansion and contraction of Sahara Desert from 1980 to 1990. *Science* **1991**, *253*, 299–301.
38. Evans, J.; Geerken, R. Discrimination between climate and human-induced dryland degradation. *J. Arid Environ.* **2004**, *57*, 535–554.
39. Herrmann, S.M.; Anyamba, A.; Tucker, C.J. Recent trends in vegetation dynamics in the African Sahel and their relationship to climate. *Glob. Environ. Chang.* **2005**, *15*, 394–404.
40. Wu, W.; de Pauw, E.; Zucca, C. Use remote sensing to assess impacts of land management policies in the Ordos rangelands in China. *Int. J. Digit. Earth* **2013**, *6*, 81–102.
41. Jackson, R.D.; Huete, A.R. Interpreting vegetation indices. *Prev. Vet. Med.* **1991**, *11*, 185–200.
42. Myneni, R.B.; Nemani, R.R.; Running, S.W. Estimation of global leaf area index and absorbed par using radiative transfer models. *IEEE Trans. Geosci. Remote Sens.* **1997**, *35*, 1380–1893.
43. Knyazikhin, Y.; Martonchik, J.V.; Myneni, R.B.; Diner, D.J.; Running, S.W. Synergistic algorithm for estimating vegetation canopy leaf area index and fraction of absorbed photosynthetically active radiation from MODIS and MISR data. *J. Geophys. Res.* **1998**, *103*, 32257–32276.
44. Myneni, R.B.; Hoffman, S.; Knyazikhin, Y.; Privette, J.L.; Glassy, J.; Tian, Y.; Wang, Y.; Song, X.; Zhang, Y.; Smith, G.R.; *et al*. Global products of vegetation leaf area and fraction absorbed PAR from year one of MODIS data. *Remote Sens. Environ.* **2002**, *83*, 214–231.
45. Fang, H.; Liang, S. A hybrid inversion method for mapping leaf area index from MODIS data: Experiments and application to broadleaf and needle leaf canopies. *Remote Sens. Environ.* **2005**, *94*, 405–424.
46. Leuning, R.; Cleugh, H.A.; Zeglin, S.J.; Hughes, D. Carbon and water fluxes over a temperate Eucalyptus forest and tropical wet/dry savanna in Australia: Measurements and comparison with MODIS remote sensing estimates. *Agric. For. Meteorol.* **2005**, *129*, 151–173.
47. De Kauwe, M.G.; Disney, M.I.; Quaife, T.; Lewis, P.; Williams, M. An assessment of the MODIS collection 5 leaf area index product for a region of mixed coniferous forest. *Remote Sens. Environ.* **2011**, *115*, 767–780.
48. Richardson, A.J.; Wiegand, C.L.; Wanjura, D.F.; Dusek, D.; Steiner, J.L. Multisite analysis of spectral-biophysical data for sorghum. *Remote Sens. Environ.* **1992**, *47*, 71–82.
49. Carlson, T.N.; Ripley, D.A. On the relation between NDVI, fractional vegetation cover, and leaf area index. *Remote Sens. Environ.* **1997**, *62*, 241–251.
50. Gutman, G.; Ignatov, A. The derivation of the green vegetation fraction from NOAA/AVHRR data for use in numerical weather prediction models. *Int. J. Remote Sens.* **1998**, *19*, 1533–1543.

51. Jiménez-Muñoz, J.C.; Sobrino, J.A.; Plaza, A.; Guanter, L.; Moreno, J.; Martínez, P. Comparison between fractional vegetation cover retrievals from vegetation indices and spectral mixture analysis: Case study of PROBA/CHRIS data over an agricultural area. *Sensors* **2009**, *9*, 768–793.
52. Zhang, X.; Liao, C.; Li, J.; Sun, Q. Fractional vegetation cover estimation in arid and semi-arid environments using HJ-1 satellite hyperspectral data. *Int. J. Appl. Earth Obs. Geoinf.* **2012**, doi:10.1016/j.jag.2012.07.003.
53. Kallel, A.; le Hégarat-Mascle, S.; Ottlé, C.; Hubert-Moy, L. Determination of vegetation cover fraction by inversion of a four-parameter model based on isoline parametrization. *Remote Sens. Environ.* **2007**, *111*, 553–566.
54. Sirikul, N. Comparison of MODIS Vegetation Index Products with Biophysical and Flux Tower Measurements. Ph.D. Dissertation, University of Arizona, Tucson, AZ, USA, 2006; p. 197.
55. Matthew, M.W.; Adler-Golden, S.M.; Berk, A.; Richtsmeier, S.C.; Levine, R.Y.; Bernstein, L.S.; Acharya, P.K.; Anderson, G.P.; Felde, G.W.; Hoke, M.P.; *et al*. Status of atmospheric correction using a MODTRAN4-based algorithm. *Proc. SPIE* **2000**, *4049*, 199–207.
56. Perkins, T.; Adler-Golden, S.; Matthew, M.; Berk, A.; Anderson, G.; Gardner, J.; Felde, G. Retrieval of Atmospheric Properties from Hyper and Multispectral Imagery with the FLAASH Atmospheric Correction Algorithm. *Proc. SPIE* **2005**, 5979, doi: 10.1117/12.626526.
57. Wu, W.; de Pauw, E.; Hellden, U. Assessing woody biomass in African tropical savannas by multiscale remote sensing. *Int. J. Remote Sens.* **2013**, *34*, 4525–4549.
58. Price, J.C.; Bausch, W.C. Leaf area index estimation from visible and near-infrared reflectance data. *Remote Sens. Environ.* **1995**, *52*, 55–65.
59. Gitelson, A.A.; Wardlow, B.D.; Keydan, G.P.; Leavitt, B. An evaluation of MODIS 250-m data for green LAI estimation in crops. *Geophys. Res. Lett.* **2007**, *34*, L20403.
60. Wang, Q.; Adiku, S.; Tenhunen, J.; Granier, A. On the relationship of NDVI with leaf area index in a deciduous forest site. *Remote Sens. Environ.* **2005**, *94*, 244–255.